Monatshefte für Chemie - Chemical Monthly (2018) 149:1389–1400
https://doi.org/10.1007/s00706-018-2184-0

ORIGINAL PAPER

Theoretical study on the elimination kinetics in the gas phase of allyl methyl compounds

Ahmad Reza Oliaey[1] · Abolfazl Shiroudi[2] · Ehsan Zahedi[3] · Michael S. Deleuze[4]

Received: 15 November 2017 / Accepted: 14 March 2018 / Published online: 27 June 2018

Abstract

The thermal decomposition kinetics of allyl methyl amine, allyl methyl ether, and allyl methyl sulfide in the gas phase has been studied theoretically using the M06-2*x*/aug-cc-pVTZ quantum chemical approach. The observed activation parameters are consistent with a concerted unimolecular mechanism involving a non-planar cyclic six-membered transition state. Based on the optimized ground state geometries, a natural bond orbital analysis of donor–acceptor interactions reveals that the stabilization energies corresponding to the electronic delocalization from the lone-pair (LP) non-bonding orbitals on the heteroatom to the neighboring σ^*_{C2-C3} antibonding orbitals decrease from allyl methyl amine to allyl methyl sulfide. This delocalization fairly explains the increase of occupancies of LP orbitals on the heteroatom from allyl methyl sulfide to allyl methyl amine. The results also suggest that the kinetics of the thermolysis of the studied compounds are dominated by LP $\rightarrow \sigma^*$ electronic delocalization effects. Analysis of bond order, bond indices, and synchronicity parameters demonstrates that these reactions proceed through a concerted and slightly asynchronous mechanism.

Graphical abstract

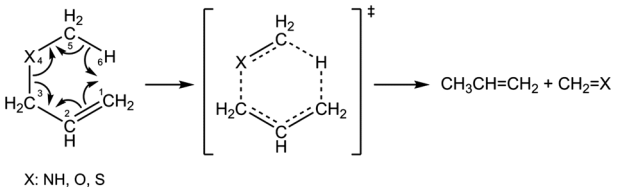

Keywords Decomposition · Energy barriers · Chemical kinetics · Reaction mechanisms · NBO · RRKM theory

Introduction

The unimolecular homogeneous elimination kinetics of allyl methyl amine (*N*-allyl-*N*-methylamine, compound **1**), allyl methyl ether (compound **2**), and allyl methyl sulfide (compound **3**) in the gas phase has generally been assumed to proceed through a concerted 1,5-H-shift retro-"ene" type mechanism involving a six-membered cyclic transition state [1–4], which yields propene as the principal observed product [1] (Scheme 1), together with methylene amine, formaldehyde, or thioformaldehyde as secondary products, respectively. Substituent effects on the corresponding reaction rates suggest that there are significant differences in the degree of concertedness of the various transition states [4].

Electronic supplementary material The online version of this article (https://doi.org/10.1007/s00706-018-2184-0) contains supplementary material, which is available to authorized users.

✉ Abolfazl Shiroudi
abolfazl.shiroudi@uhasselt.be

[1] Chemistry Department, Tonekabon Branch, Islamic Azad University, Tonekabon, Iran

[2] Young Researchers and Elite Club, East Tehran Branch, Islamic Azad University, Tehran, Iran

[3] Chemistry Department, Shahrood Branch, Islamic Azad University, Shahrood, Iran

[4] Center of Molecular and Materials Modelling, Hasselt University, Agoralaan, Gebouw D, 3590 Diepenbeek, Belgium

Scheme 1

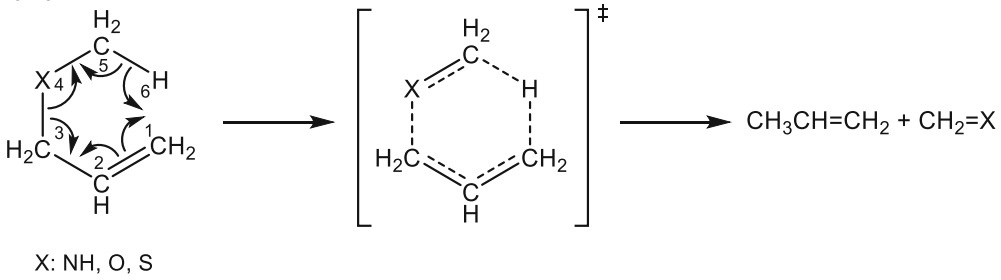

In the course of preceding experimental work [1–4], it became evident that the activation energies for the thermally induced unimolecular decomposition of compounds **1–3** via Scheme 1 are strongly sensitive towards replacement of the NH group by oxygen and sulfur atoms (compounds **2** and **3**, respectively). The effect of the nature of the X group should provide useful information with regard to the amount of charge separation in the transition state [2]. Systematic kinetic studies on these compounds should, therefore, yield useful information on the extent of charge separation, i.e., non-synchronism, in the relevant transition state [1].

Vitins and Egger [1], Kwart et al. [3], as well as Martin et al. [4] have experimentally measured kinetic rate constants for the studied reactions at temperatures ranging from 329 to 537 °C.

The gas-phase unimolecular thermal decomposition of *N*-allyl-*N*-methylamine (AMA) was investigated by Vitins and Egger [1] at temperatures ranging from 329 to 421 °C. The principal products are propene and methylenearnine. First-order rate constants, calculated using the internal standard method, fit the Arrhenius relationship as follows:

$$k_1(\mathrm{s}^{-1}) = 10^{(11.37\pm0.56)}\ \exp[-(181.5 \pm 6.78\ \mathrm{kJ/mol})/RT]\,.$$

Kinetic rate constants for the thermal decomposition of allyl methyl ether have been studied by Kwart et al. [3] in the gas phase at temperatures comprised between 452 and 537 °C. The experimentally determined first-order rate constants, using the internal standard technique, fit the Arrhenius relationship as follows:

$$k_2(\mathrm{s}^{-1}) = 10^{(11.09\pm0.02)}\exp[-(174.05 \pm 2.51\ \ \mathrm{kJ/mol})/RT].$$

Martin et al. [4] have experimentally measured kinetic rate constant for the pyrolysis reaction of allyl methyl sulfide in a stirred-flow system at temperatures within the range 376–418 °C and initial pressures between 2 and 15 Torr. A least-square fit of the rate coefficient in the form of the Arrhenius equation produced the following relationship:

$$k_3(\mathrm{s}^{-1}) = 10^{(11.23\pm0.25)}\ \exp[-(160 \pm 3\ \mathrm{kJ/mol})/RT].$$

The Arrhenius parameters are consistent with a unimolecular mechanism involving six-centered cyclic transition states yielding propene and thioaldehyde.

The kinetic rate constants for the unimolecular decomposition of compounds **1–3** in the gas phase exhibit positive temperature dependences which are equivalent to Arrhenius activation energies of (181.50 ± 6.78) [1], (174.05 ± 2.51) [3], and (160 ± 3) kJ/mol [4], respectively.

Although the reaction kinetics of the decomposition processes of compounds **1–3** has been investigated experimentally in the gas phase [1, 3, 4], there is not any theoretical and experimental data concerning the role played by effective parameters like resonance effects on the transition states, or stabilization and resonance effects on the occupancies of bonding and antibonding orbitals.

The aim of this study is to calculate on quantum chemical grounds the activation energies and kinetic rate constants for the thermally induced decomposition of compounds **1–3**, and to unravel the molecular mechanism of these reactions. Transition State Theory (TST) [5–12] in conjunction with the M06-2*x* [13] exchange–correlation functional and Dunning's augmented correlation consistent polarized valence basis set of triple zeta quality (aug-cc-pVTZ) [14] will be used to calculate kinetic rate constants in the high-pressure limit. In addition, their fall-off behavior will be investigated at lower pressures by means of statistical Rice–Ramsperger–Kassel–Marcus (RRKM) theory [15–17], to unravel the available experimental data [2–4], at temperature ranging from 329 to 537 °C. Finally, results obtained by means of Natural Bond Orbital (NBO) analyses [18, 19] will be examined for the purpose of supplying further qualitative chemical insights into the studied reaction mechanisms.

Results and discussion

The geometrical characteristics of the reactants (R), transition states (TS), and products (P) of the studied reactions are supplied at the M06-2*x*/aug-cc-pVTZ theoretical level in Table 1 (see Scheme 1 for atom numbering). Inspection of the geometries of the transition states on the reaction pathway for the decomposition of compounds **1**–**3** show that the reaction proceeds via a concerted 1,5-H-shift retro-"ene" type mechanism. The transition states correspond to six-membered cyclic structures. The most significant geometrical change is observed for the C_1–H_6 bond, which shrinks by $\sim$ 1.4 to $\sim$ 1.6 Å in the transition state, compared with the structure of the reactants. The C_3–X_4 and C_5–H_6 bond lengths correspondingly increase by $\sim$ 0.4 Å, indicating cleavage of these bonds in the transition states, while the variations in the C_2–C_3 bond length, which decreases from 1.503–1.508 to 1.374–1.382 Å, reveal a conversion of this chemical bond from a single to a double bond (see Fig. 1).

The dihedral angles that are supplied in Table 1 indicate correspondingly a rotation of the C_5–H_6 bond by $\sim$ 50°, $\sim$ 78°, and $\sim$ 80°, when X = NH, O, and S, respectively. These results suggest that the transition states for the thermally induced unimolecular decomposition of compounds **1**–**3** are non-planar. The imaginary frequencies characterizing these transition states amount to 1227.2*i*, 1159.3*i*, and 1114.9*i* cm^{-1} when X = NH, O, and S, respectively.

According to Hammond's postulate, the transition state of a reaction resembles more the structure of the species (reactant or product) to which it is closer in free energy [20]. This resemblance is usually quantified in terms of the position of the transition structure along the reaction coordinate, n_T, a parameter which reads, according to the definition by Agmon and Levine [21]:

$$n_T = \frac{1}{2 - (\Delta G^o / \Delta G^{\dagger})}. \quad (1)$$

The n_T values for the thermally induced unimolecular decomposition of compounds **1**–**3** are equal to 0.50, 0.48, and 0.60, respectively. The similarity between the transition states and products increases in the order X = S, X = NH, and X = O. The unimolecular decomposition of allyl methyl ether (compound **2**) is found to be exergonic ($\Delta G < 0$) in agreement with the geometrical feature of the transition state which structurally resembles that of the reactant, while the unimolecular decomposition of allyl methyl sulfide (compound **3**) is characterized by a transition state which is structurally closer to the products than to the reactant, and is expected, therefore, to be endoergic. Accordingly, the relationship between the earliness of the transition states and the ΔG values is very well observed.

Activation enthalpies ($\Delta H^{\dagger}$), activation Gibbs free energies ($\Delta G^{\dagger}$), and reaction energies (ΔH and ΔG) at 298 K for the unimolecular decomposition of allyl methyl amine (*N*-allyl-*N*-methylamine, compound **1**), allyl methyl ether (compound **2**), and allyl methyl sulfide (compound **3**) are summarized in Tables 2 and 3. In line with the available experimental Arrhenius activation energies [2–4], the M06-2*x*/aug-cc-pVTZ calculations show that the unimolecular decomposition of compounds **1**–**3** is an endothermic process ($\Delta H \approx$ 52.46, 30.0, and 103.36 kJ/mol, when X = NH, O, and S, respectively)

Table 1 Structural parameters for all the stationary points which are involved in the unimolecular decomposition of *N*-allyl-*N*-methylamine (compound **1**), allyl methyl ether (compound **2**), and allyl methyl sulfide (compound **3**) (results obtained using the M06-2*x*/aug-cc-pVTZ approach)

Bond	Species								
	1			**2**			**3**		
	R	*TS*	*P*	*R*	*TS*	*P*	*R*	*TS*	*P*
Bond lengths/Å									
r (C_1–C_2)	1.323	1.399	1.495	1.322	1.399	1.495	1.323	1.413	1.495
r (C_2–C_3)	1.508	1.382	1.324	1.503	1.381	1.324	1.503	1.374	1.324
r (C_3–X_4)	1.448	1.979	–	1.404	1.876	–	1.809	2.306	–
r (X_4–C_5)	1.455	1.346	1.261	1.409	1.284	1.196	1.808	1.667	1.600
r (C_5–H_6)	1.096	1.385	–	1.093	1.366	–	1.087	1.492	–
d (C_1–H_6)	2.776	1.359	1.089	2.807	1.362	1.089	2.852	1.279	1.089
Dihedral angles/°									
φ (C_1–C_2–C_3–X_4)	7.6	59.7	–	− 8.2	− 65.4	–	− 9.5	− 72.3	–
φ (C_3–X_4–C_5–H_6)	− 54.7	− 4.3	–	56.6	− 21.4	–	61.1	− 18.5	–

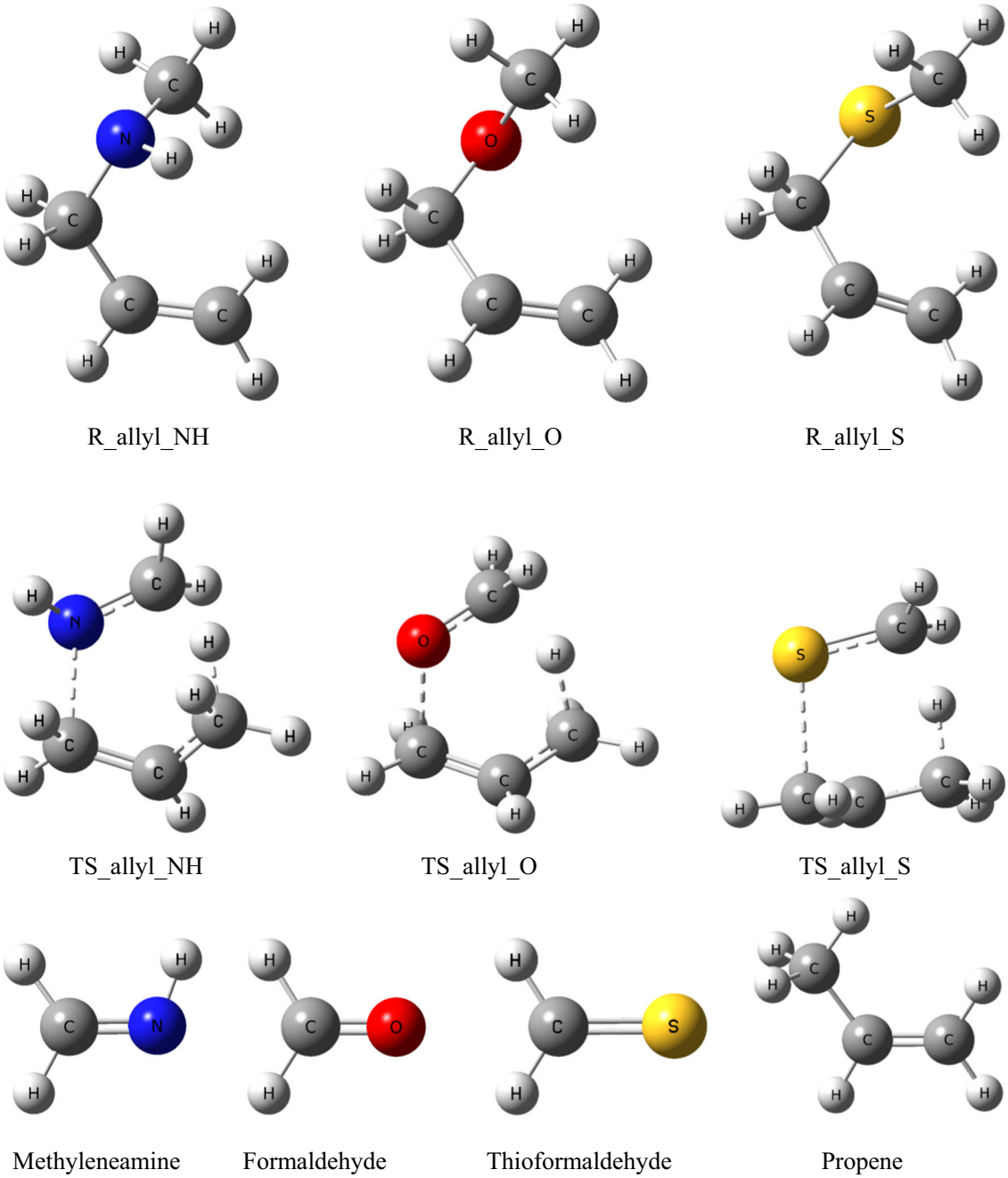

Fig. 1 Stationary points (reactants, transition states, and products) for the unimolecular decomposition of compounds **1–3**

Table 2 Reaction energies, reaction enthalpies, and Gibb's free reaction energies for the thermolysis of compounds **1–3** at the M06-2*x*/aug-cc-pVTZ level of theory (all results are given in kJ/mol)

Reaction	Parameter		
	ΔE_{0K}	$\Delta H°_{298K}$	$\Delta G°_{298K}$
Allyl methyl amine → $CH_3CH{=}CH_2 + CH_2{=}NH$	47.83	52.46	0.90
Allyl methyl ether → $CH_3CH{=}CH_2 + CH_2{=}O$	25.26	30.00	− 19.14
Allyl methyl sulfide → $CH_3CH{=}CH_2 + CH_2{=}S$	100.14	103.36	56.07

Table 3 Activation energies, activation enthalpies, Gibb's free activation energies, and entropies for the thermolysis of compounds **1–3**, at the M06-2*x*/aug-cc-pVTZ theoretical level (P = 1 atm)

Reaction	Parameter				
	$\Delta E^{\dagger}_{0K}$	$\Delta H^{\circ\dagger}_{298K}$	$\Delta G^{\circ\dagger}_{298K}$	$\Delta S^{\circ\dagger}_{298K}$	Literature $\Delta E^{\dagger}$
Allyl methyl amine → TS1	218.30	216.66	220.19	− 11.86 (− 41.40)[a]	(181.50 ± 6.78)[a]
Allyl methyl ether → TS2	195.50	193.41	198.29	− 16.36 (− 48.53 ± 2.93)[b]	(174.05 ± 2.51)[b]
Allyl methyl sulfide → TS3	164.37	162.12	167.59	− 18.36 (− 44.70)[c]	(160.0 ± 3.01)[c]

Energies (enthalpies) and entropies are given in kJ/mol and J/mol/K, respectively. Experimental activation entropies have been calculated at 375 °C

Experimental values: [a]Ref. [2]; [b]Ref. [3]; [c]Ref. [4]

which are shown in Fig. 2. At ambient temperature and pressure, the Gibbs free reaction energy for the unimolecular decomposition of allyl methyl ether (compound **2**) is negative; hence, this reaction is an exoergic and spontaneous process, while the Gibbs free reaction energies for the unimolecular decomposition of *N*-allyl-*N*-methylamine (compound **1**) and allyl methyl sulfide (compound **3**) are positive; therefore, these reactions are endoergic and non-spontaneous processes. Upon inspecting the energy profiles supplied in Table 2, it appears that the production of the $CH_3CH = CH_2 + CH_2 = O$ species will be the thermodynamically most favored process.

At ambient temperature and pressure, the thermal decomposition reactions of compounds **1–3** are endothermic ($\Delta H^{\dagger} > 0$) and endergonic (non-spontaneous) processes ($\Delta G^{\dagger} > 0$). The activation entropies of the unimolecular decomposition of compounds **1–3** amount to − 11.86, − 16.36, and − 18.36 J/mol/K, respectively (Table 3). These negative values for the activation entropies are in line with the concerted nature of the reaction mechanism.

The activation energy barrier for the thermally induced unimolecular decomposition of compound **3** is, therefore, 30.97 and 53.97 kJ/mol lower than the barriers for the unimolecular decomposition of compounds **1** and **2**, respectively (Table 3). Such a difference in the obtained activation energies and Gibb's free activation energies for these unimolecular reaction pathways **1–3** indicates that the formation of thioformaldehyde species (P3) will be kinetically favored over the formation of methyleneamine (P1) and formaldehyde (P2).

The thermally induced unimolecular decomposition of compounds **1–3** in the gas phase correspond to concerted, six-center, and homolytic reaction processes. Upon inspecting Table 3, it appears that the activation enthalpies ($\Delta H^{\dagger}$) and activation free energies ($\Delta G^{\dagger}$) of all investigated chemical pathways are positive; therefore, activation processes require excess energy, and are not spontaneous. Moreover, activation entropies ($\Delta S^{\dagger}$) are negative but rather small. The obtained $\Delta H^{\dagger}$ and $\Delta G^{\dagger}$ parameters are, therefore, very close to the ΔE_{0K} values.

We also employed the distortion–interaction model to investigate the origins of reactivity and selectivities in a variety of organic and organometallic reactions [22–30]. Although this model was originally conceived for bimolecular reactions, it can also be applied to unimolecular reactions [31–33]. The total activation energy ($\Delta E^{\dagger}$) along the reaction coordinate is devolved into the distortion (strain) energy ($\Delta E^{\dagger}_{dist}$) of the reactants that become increasingly deformed as the reaction proceeds and interaction energy ($\Delta E^{\dagger}_{int}$) of the two distorted reactants (see Fig. 3). This model is directly used for transition states in bimolecular reactions [34] as follows:

$$\Delta E^{\dagger} = \Delta E^{\dagger}_{dist} + \Delta E^{\dagger}_{int}, \quad (2)$$

where $\Delta E^{\dagger}_{dist}$ is defined as the energy which is needed to deform the reactants from their equilibrium geometries to the geometries they adopt in the corresponding transition state, and $\Delta E^{\dagger}_{int}$ is the energy change upon interaction of the two distorted fragments [35–37].

In general, $\Delta E^{\dagger}_{dist}$ is a positive value that is destabilizing, and consequently a factor that gives rise to the occurrence of a reaction barrier, while in most cases, $\Delta E^{\dagger}_{int}$ is a negative value which is stabilizing, and hence a factor that counteracts the strain term $\Delta E^{\dagger}_{dist}$ and causes the eventual height of the reaction barrier to become lower than if strain would be the only factor [34].

Based on a careful and chemically meaningful fragmentation scheme, unimolecular reactions can be studied as well by this model [34]. A straightforward way of dealing with this situation is to equate the activation energy ($\Delta E^{\dagger}$) and the activation strain ($\Delta E^{\dagger}_{dist}$), because there is no second reactant to interact with, that is: $\Delta E^{\dagger} = \Delta E^{\dagger}_{dist}$. A more insightful approach is to identify, if possible, two

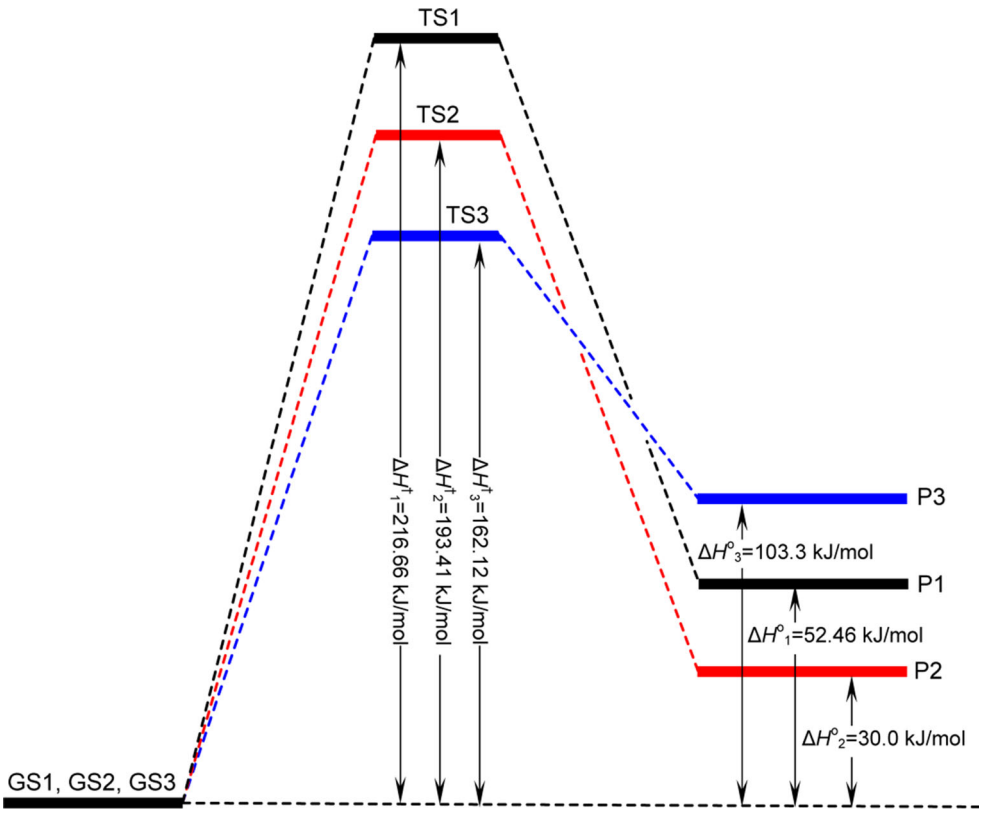

Fig. 2 Energy profile for the unimolecular thermal decomposition of compounds **1**–**3**

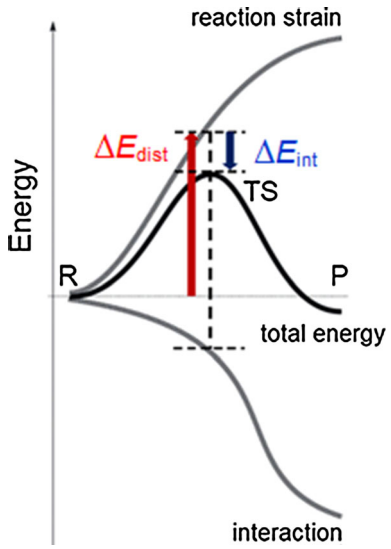

Fig. 3 Activation strain–distortion/interaction model [37]

fragments in the rearranging reactant that display a clear relative movement with respect to each other.

Distortion–interaction energy analysis of the transition states was first used to explain the reactivity trends of these unimolecular reactions, and the results are shown in Table 4. M06-2*x*/aug-cc-pVTZ calculations of the thermal decomposition of Allyl methyl amine (compound **1**) to propene and methyleneamine give a distortion energy of 237.11 kJ/mol and an interaction energy of − 59.53 kJ/mol. For the reaction with allyl methyl ether (compound **2**), the distortion energy in transition state TS2 is 24.85 kJ/mol higher than that in transition state TS1, and the interaction energy for transition state TS2 is 8.32 kJ/mol higher than TS1. For the unimolecular decomposition reaction of allyl methyl sulfide (compound **3**), the distortion energy is 278.49 kJ/mol which is 16.53 kJ/mol higher than that for allyl methyl ether. Moreover, the interaction energy for transition state TS3 is 7.5 kJ/mol higher than TS2.

Compared with the unimolecular decomposition reactions of compounds **1**–**3**, the lowest distortion energy and lower interaction energy of transition state TS1 result in the

Table 4 Distortion–interaction energy analysis (in kJ/mol) of the transition states of the unimolecular reactions (**1**)–(**3**) by the M06-2*x* theoretical method (M06-2*x*/aug-cc-pVTZ results)

Substrate	Parameter			
	TS	$\Delta E^{\dagger}_{dist}$	$\Delta E^{\dagger}_{int}$	$\Delta E^{\dagger}$
Allyl methyl amine	TS1	237.11	− 59.53	177.58
Allyl methyl ether	TS2	261.96	− 51.21	210.75
Allyl methyl sulfide	TS3	278.49	− 43.71	234.78

highest activation energy. The highest distortion energy of transition state TS3 contributes to the lowest activation energy. Distortion–interaction energy analysis of the transition states indicates that the reactivity difference of the studied chemical reactions (**1**)–(**3**) is controlled by both the distortion energy and interaction energy.

A quantitative measure of the extent of bond breaking or of bond forming processes along a chemical reaction pathway is possible using the concept of bond order (*B*) [12, 18, 38]. This concept has enabled detailed investigations of the molecular mechanism of many chemical reactions [38]. In the present work, Wiberg bond indices [39] have been calculated according to an NBO analysis [40], to unravel the nature of the reaction pathway. There are several bonds which form and break during the fragmentation process and the global nature of the thermolysis reaction can be monitored using the synchronicity (S_y) index introduced by Moyano et al. [41]. This index is defined as follows:

$$S_y = 1 - \frac{\left[\sum_{i=1}^{n} \frac{|\delta B_i - \delta B_{av}|}{\delta B_{av}}\right]}{2n-2}, \quad (3)$$

where n is the number of chemical bonds that are involved directly in the studied reactions. The relative variation of the bond index (δB_i) for a bond i at the level of the transition state is given by

$$\delta B_i = \frac{B_i^{TS} - B_i^R}{B_i^P - B_i^R}, \quad (4)$$

where the superscripts *R*, *TS*, and *P* represent the reactant, the transition state, and the products, respectively. The variation in bond order is evaluated as $\%EV = \delta B_i \times 100$. The average value in the change of bond orders is calculated according to

$$\delta B_{av} = \frac{1}{n}\sum_{i=1}^{n} \delta B_i. \quad (5)$$

The synchronicity parameter S_y varies in between 0 and 1: a value of $S_y = 0$ indicates a fully asynchronic processes, whereas a value of $S_y = 1$ shows on the contrary a fully concerted synchronic process [42].

Bond indices were computed for the chemical bonds that are involved in the studied reaction pathways, i.e., the C_1–X_2, C_2–X_3, C_3–X_4, X_4–X_5, C_5–X_6, and C_1–X_6 bonds (see Scheme 1 for atom numbering). All other bonds remain almost unaltered. The obtained Wiberg bond indices B_i for the identified stationary points on the reaction pathway enable us (Table 5) to examine the reaction progress and to evaluate the position of the transition states in between the reactants and products. The unimolecular gas-phase decomposition of compounds **1**–**3** implies the cleavage of the C_3–X_4 and C_5–X_6 bonds to yield products that lie at 45.19–47.70, 10.46–25.10, and 94.98–99.99 kJ/mol above the reactants when X = NH, O, and S, respectively. Transition states result from the elongation and cleavage of the C_3–X_4 and C_5–X_6 bonds and the simultaneous decrease of the C_1–H_6 bond length, which accompanies the formation of a C–C bond (Table 5).

Wiberg bond indices show that, for the thermal unimolecular decomposition of compounds **1**–**3**, the C_1–C_2 double bond formation ($\%EV$ = 64.7–73.8%) progresses faster than the breaking of the C_3–X_4 and C_5–X_6 bonds, which is intermediate in the reaction coordinate ($\%EV$ = 53.03–57.20% and $\%EV$ = 51.72–62.86%, respectively). The formation of the X_4–X_5 double bond is slower ($\%EV$ = 39.71–45.96%) for all studied reaction channels. The synchronicity values of the thermolysis of compounds **1**–**3** are around ~ 0.93, which indicates that the studied channels can be regarded as concerted and slightly asynchronous.

Delocalization of the electron density between occupied [bonding or lone pair (LP)] Lewis-type NBO orbitals and empty (antibonding and Rydberg) non-Lewis NBO orbitals [19, 43, 44] imply stabilizing donor–acceptor interactions. The energies of these interactions can be evaluated according to second-order perturbation energies (E_2) [12]. According to our NBO analysis (Table 6), the charge transfer between the LPs of the proton acceptor and the antibonding orbitals of the proton donor is the strongest effect.

The NBO analysis shows that the HOMO–LUMO energy gap for compounds **1**–**3** amounts to 7.73, 8.62, and 7.47 eV, respectively. This gap decreases in parallel with the decrease of the electronegativity (Table 6) of the X group (see Scheme 1).

Furthermore, the NBO results demonstrate that because of the decrease of the $LP(e)_{X4} \rightarrow \sigma^*_{C2-C3}$ resonance energy, the barrier height (ΔE_o) for the thermally induced decomposition of allyl methyl compounds decreases from compounds **1**–**3**. This fact could explain that the aromatic character in the corresponding reaction TS structures of compound **1** is more than compound **2** and compound **2** is more than compound **3**. The $LP(e)_{X4}$ lone pairs occupancy correspondingly increases, whereas the σ^*_{C2-C3} antibonding orbital occupancy decreases. The $LP(e)_{X4}$ lone pairs occupancies in compounds **1**–**3** amount to 1.915, 1.924, and 1.925, respectively, while the σ^*_{C2-C3} antibonding occupancies in compounds **1**–**3** are equal to 0.037, 0.033, and 0.032, respectively. The occupancies of the σ_{C2-C3} bonds increase correspondingly in the opposite order (Table 6). This trend explains the easier thermal decomposition of allyl methyl sulfide (compound **3**) (i.e., the relatively lower energy barrier of this reaction) compared

Table 5 Bond-order analysis of the stationary points that are involved in the thermal decomposition of allyl methyl amine (reaction **1**), allyl methyl ether (reaction **2**), and allyl methyl sulfide (reaction **3**); M06-2*x*/aug-cc-pVTZ results obtained according to an NBO analysis

Reaction	Bond								
		C_1–X_2	C_2–X_3	C_3–X_4	X_4–X_5	C_5–X_6	C_1–X_6	δB_{av}	S_y
1	$B_i(R)$	1.982	1.021	1.01	1.008	0.939	0.001	0.510	0.930
	$B_i(TS)$	1.381	1.465	0.477	1.415	0.440	0.467		
	$B_i(P)$	1.053	1.984	0.000	2.034	0.000	0.941		
	$\%EV$	64.70	46.13	53.03	39.71	53.13	49.52		
2	$B_i(R)$	1.983	1.024	0.936	0.929	0.946	0.001	0.511	0.926
	$B_i(TS)$	1.375	1.459	0.419	1.332	0.457	0.463		
	$B_i(P)$	1.053	1.984	0.000	1.937	0.000	0.941		
	$\%EV$	65.32	45.37	55.25	39.99	51.72	49.14		
3	$B_i(R)$	1.984	1.030	1.018	1.029	0.931	0.001	0.585	0.932
	$B_i(TS)$	1.296	1.532	0.436	1.501	0.346	0.554		
	$B_i(P)$	1.053	1.984	0.000	2.055	0.000	0.941		
	$\%EV$	73.83	52.58	57.20	45.96	62.86	58.73		

Wiberg bond indices (B_i), relative evolution of the bond indices through the reaction coordinate ($\%EV$), average variation of the bond indices (δB_{av}), and synchronicity parameter (S_y) are shown

Table 6 NBO resonances energies (E_2) in kJ/mol which are associated with σ_{C1-C2} to σ^*_{C2-C3} delocalization effects, and HOMO–LUMO energy gaps in the ground state geometries of allyl methyl amine (compound **1**), allyl methyl ether (compound **2**), and allyl methyl sulfide (compound **3**)

	M06-2*x*/aug-cc-pVTZ		
	1 (X = NH)	**2** (X = O)	**3** (X = S)
Occupancies			
σ_{C1-C2}	1.992	1.991	1.992
σ^*_{C2-C3}	0.009	0.008	0.009
σ_{C2-C3}	1.986	1.987	1.988
σ^*_{C2-C3}	0.037	0.033	0.033
$LP(e)_{X4}$	1.915	1.924	1.925
Resonances energies (E_2)			
$\sigma_{C1-C2} \rightarrow \sigma^*_{C2-C3}$	4.31	4.02	5.69
$LP(e)_{X4} \rightarrow \sigma^*_{C2-C3}$	44.64	37.69	27.28
HOMO–LUMO energies (a.u.) and gap (eV)			
HOMO	− 0.288	− 0.320	− 0.280
LUMO	− 0.004	− 0.004	− 0.005
HOMO–LUMO gap	0.284 (7.73 eV)	0.317 (8.62 eV)	0.275 (7.47 eV)

to *N*-allyl-*N*-methylamine (compound **1**) and allyl methyl ether (compound **2**).

Unimolecular kinetic rate constants for the thermally induced decomposition of compounds **1**–**3** are supplied in Table 7 at the experimentally considered temperatures [2–4], considering a pressure of 1 bar. These rate constants are the results of TST and RRKM calculations performed upon the M06-2*x*/aug-cc-pVTZ energy barriers and densities of states. Further RRKM data obtained at lower and higher pressures are given at the same temperatures in Tables S1a–S1d of the "Electronic supplementary material," (ESM). The theoretical kinetic rate constants that were obtained at a pressure of 1 bar for the thermal decomposition of allyl methyl sulfide (reaction **3**) do not differ by more than three orders of magnitude from experiment.

For chemical reaction (**1**), the calculated kinetic rate constants using the TST and RRKM models at 375 °C are very close to the available experimental data. This is due to error cancellation between an underestimation of rate constant due to the higher calculated activation energy and an overestimation of rate constant because of the less

Table 7 Unimolecular kinetic rate constants (in s^{-1}) for the decomposition of allyl methyl amine (reaction **1**), allyl methyl ether (reaction **2**), and allyl methyl sulfide (reaction **3**)

T/°C	Pathway					
	TST			RRKM		
	Reaction 1 [R1 → P1]	Reaction 2 [R2 → P2]	Reaction 3 [R3 → P3]	Reaction 1 [R1 → P1]	Reaction 2 [R2 → P2]	Reaction 3 [R3 → P3]
329	1.52×10^{-5}	7.13×10^{-4}	1.84×10^{-1}	1.15×10^{-5}	5.43×10^{-4}	1.43×10^{-1}
375	2.68×10^{-4} (2.67×10^{-4})[a]	9.21×10^{-3} (3.87×10^{-4})[b]	1.56×10^{0} (7.5×10^{-3})[c]	2.12×10^{-4}	7.29×10^{-3}	1.26×10^{0}
400	1.09×10^{-3}	3.21×10^{-2}	4.42×10^{0}	8.74×10^{-4}	2.59×10^{-2}	3.62×10^{0}
450	1.35×10^{-2}	3.01×10^{-1}	2.88×10^{1}	1.12×10^{-2}	2.51×10^{-1}	2.42×10^{1}
500	1.21×10^{-1}	2.13×10^{0}	1.48×10^{2}	1.03×10^{-1}	1.82×10^{0}	1.27×10^{2}
537	5.19×10^{-1}	7.79×10^{0}	4.38×10^{2}	4.47×10^{-1}	6.74×10^{0}	3.81×10^{2}

These data were obtained at $P = 1$ bar using TST and RRKM theories, at the M06-2*x*/aug-cc-pVTZ level of theory

Experimental values: [a]Ref. [2]; [b]Ref. [3]; [c]Ref. [4]

negative value of calculated activation entropy. While in the chemical reaction (**3**), calculated rate constants by means of the TST and RRKM models at the same temperature are about 10^3 times larger than the experimental value. In this case, the calculated activation energy is in good agreement with the experimental value. Therefore, less negative value of calculated activation entropy leads to the overestimation of the rate constants.

Whatever the considered temperatures, the unimolecular rate constant for reaction (**3**) is larger than that obtained for the chemical pathways **1** and **2**. This observation is in line with a reduction of the activation energy barrier by 30.96 and 53.97 kJ/mol, respectively. As is to be expected in view of the involved energy barriers, these kinetic rate constants increase smoothly with increasing temperatures. As a result, these energy results indicate that reaction (**3**) is the most favorable channel from the kinetic viewpoint.

An Arrhenius plot (Fig. 4) of the kinetic rate constants which were obtained by means of RRKM theory for the chemical reactions (**1**)–(**3**) clearly confirms that the production of the $CH_3CH{=}CH_2 + CH_2{=}S$ (**P3**) species will be the most efficient process under atmospheric pressure and at the studied temperatures. The same observation can be made for pressures ranging from 10^{-12} to 10^{2} bars

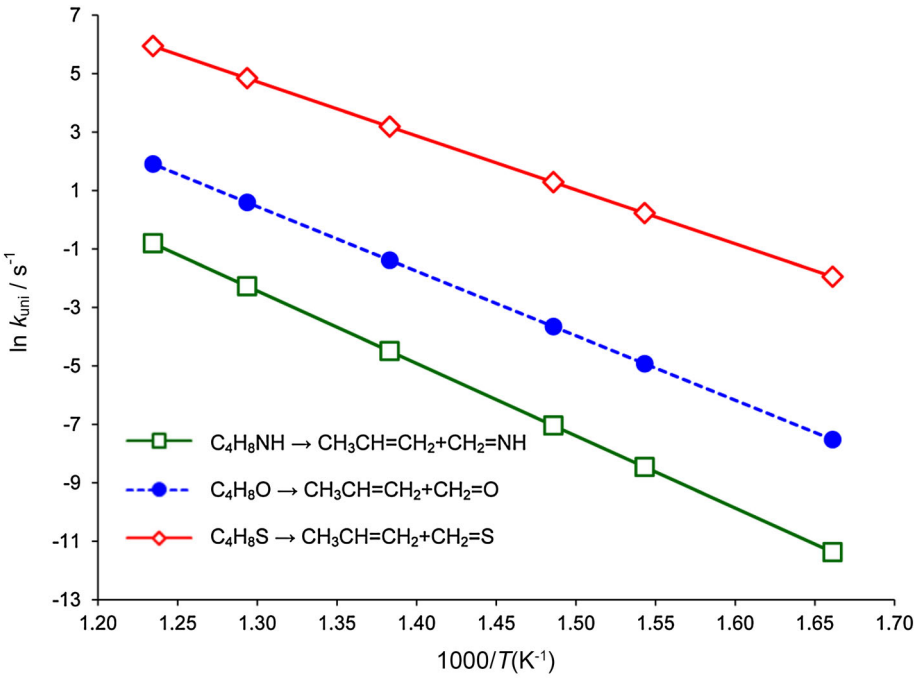

Fig. 4 Arrhenius plot of the RRKM unimolecular rate constants which were obtained for the thermolysis of allyl methyl amine (C_4H_8NH), allyl methyl ether (C_4H_8O), and allyl methyl sulfide (C_4H_8S); results obtained upon M06-2*x*/aug-cc-pVTZ data

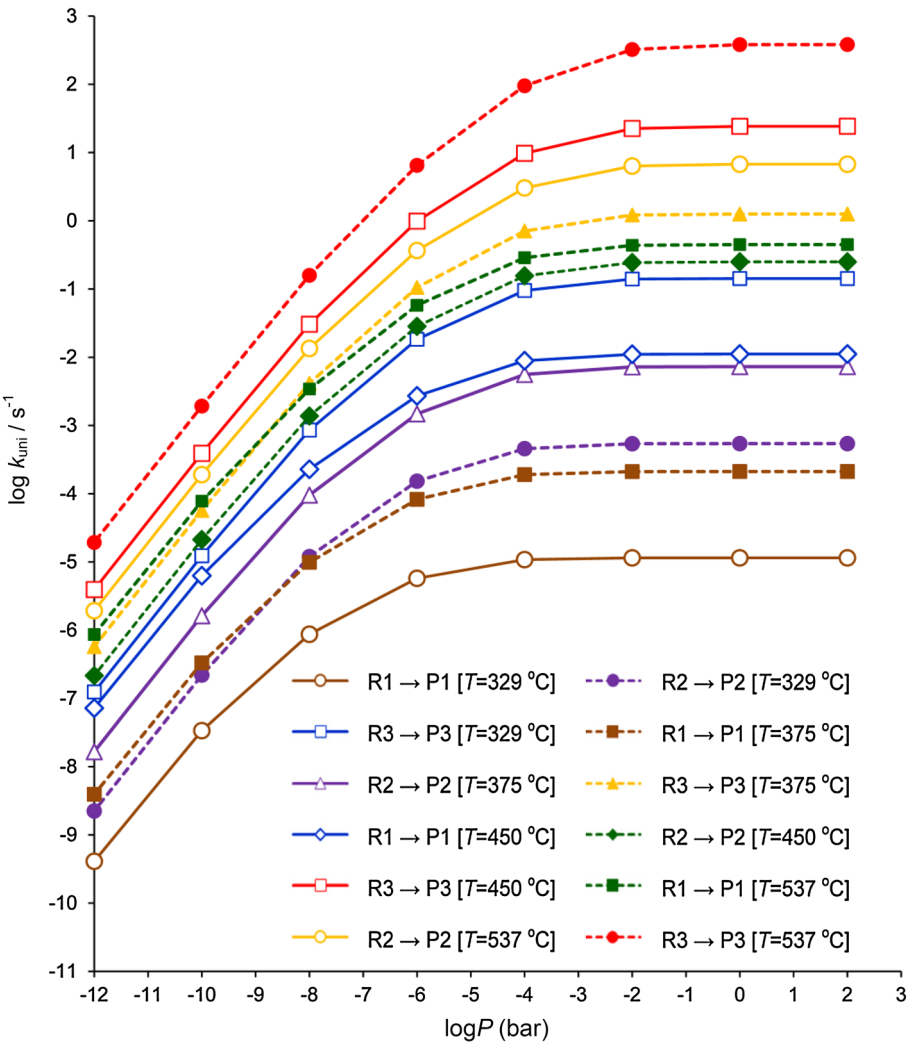

Fig. 5 Pressure dependence of the kinetic rate constants for the thermally induced decomposition processes of allyl methyl amine (reaction **1**: R1 → P1), allyl methyl ether (reaction **2**: R2 → P2), and allyl methyl sulfide (reaction **3**: R3 → P3); results obtained upon M06-2*x*/aug-cc-pVTZ quantum chemical data

(Tables S1a–S1d in the Supplementary Information). In line with larger energy barriers, the thermolysis of allyl methyl amine (reaction **1**) and allyl methyl ether (reaction **2**) is characterized by much lower rate constants, by 3–4 orders of magnitude at the selected temperatures, compared with the formation of the $CH_3CH{=}CH_2$ + $CH_2{=}S$ species (reaction **3**).

Figure 4 confirms rather clearly that the production of the $CH_3CH{=}CH_2$ and $CH_2{=}S$ species (via pathway **3**) is the fastest process at all considered temperatures, down to pressures around 10^{-12} bar. The same observation can be made at much higher and lower pressures (10^{-12}–10^{2} bar) (Tables S1a–S1d of the Supplementary Information). The RRKM rate constants obtained for the unimolecular decomposition of all allyl methyl X (X = NH, O, S) compounds increase with increasing temperatures (Fig. 4 and Table 7).

The pressure dependence of the computed RRKM rate constants is depicted at 329, 375, 450, and 537 K in Fig. 5. Upon inspecting this figure, it is immediately apparent that for the thermolysis of *N*-allyl-*N*-methylamine (reaction **1**) and allyl methyl ether (reaction **2**), rather high pressures ($> 10^{-2}$ bar) are large enough to ensure a saturation of the RRKM rate constants, in comparison with the high-pressure limit (TST). In contrast, the TST approximation is no longer valid at pressures lower than 10^{-2} bar for the thermolysis of allyl methyl sulfide (reaction **3**: $C_4H_8S \rightarrow CH_3CH{=}CH_2 + CH_2{=}S$). Furthermore, detailed inspection of Table 7 shows that, at a pressure of 1 bar, the ratios between the TST and RRKM estimates of rate constants for reaction (**3**) decreases from $\sim$ 1.29 to $\sim$ 1.15 as the temperature increases from 329 to 537 °C. These differences are due to the applied tunneling corrections.

Conclusion

The thermally induced decomposition of allyl methyl amine, allyl methyl ether, and allyl methyl sulfide has been studied computationally in the gas phase at the M06-2*x*/

aug-cc-pVTZ level of theory. The obtained activation energies and unimolecular kinetic rate constants are in fair agreement with experiment. The transition states of these reactions correspond to non-planar six-membered cyclic structures. Analysis of the computed chemical pathways using synchronicity indices indicates concerted and slightly asynchronous processes. The obtained energy profiles have been supplemented with calculations of kinetic rate constants under atmospheric pressure and in the fall-off regime, by means of Transition State and RRKM theories. The RRKM calculations show in particular that exceedingly high pressures, around $\sim 10^{-2}$ bar, are necessary for restoring the validity of the TST approximation for all studied reaction channels. In line with experimental observations [2–4], the obtained kinetic rate constants show that, at temperatures ranging from 329 to 537 °C, the most efficient process is the thermal decomposition of allyl methyl sulfide into propene and thioformaldehyde. RRKM theory appears to enable semi-quantitative insights into the experimentally available kinetic rate constants [45], with discrepancies of the order of three orders of magnitude between experiment and theory.

An NBO analysis reveals that the resonance energy corresponding to the electronic delocalization from the non-bonding lone-pair (LP) orbitals on the heteroatom to the σ^*_{C2-C3} antibonding orbital decreases from allyl methyl amine (compound **1**) to allyl methyl sulfide (compound **3**). The non-bonding lone-pair orbitals occupancies on the heteroatom correspondingly increases in the following order: allyl methyl amine < allyl methyl ether < allyl methyl sulfide. The occupancies of the σ^*_{C2-C3} bonds decrease correspondingly in the opposite order. The decrease of the extent of the $LP(e)_{X4} \rightarrow \sigma^*_{C2-C3}$ delocalization fairly explains the decrease in the kinetic rate constants which is observed for the thermal decomposition of, successively, allyl methyl amine, allyl methyl ether, and allyl methyl sulfide.

Theoretical background and computational details

All the calculations reported in this study were performed using the Gaussian09 package of programs [46]. The geometries and harmonic vibrational frequencies of all stationary points (i.e., reactants, transition states, and products) involved in the reactions of interest were determined using Density Functional Theory (DFT) [47] in conjunction with the M06-2*x* functional [13] and the aug-cc-pVTZ basis set [14]. The M06-2*x* functional is usually considered to be the most suitable one for thermochemical and kinetics calculations [13]. Harmonic vibrational frequencies were computed at the M06-2*x*/aug-cc-pVTZ level for the purpose of verifying whether the identified stationary points are local energy minima or saddle points on the reaction pathways. The Intrinsic Reaction Coordinate (IRC) approach [48, 49] and to ensure that the identified transition states correctly connect the reactants and products.

In line with the temperatures at which the experiments were conducted, unimolecular rate constants for the studied reaction channels have been calculated at temperatures ranging from 329 to 537 °C and in the high-pressure limit (1 atm) by means of Transition State Theory, using the M06-2*x*/aug-cc-pVTZ activation energies. According to TST, unimolecular kinetic rate constants are given by [50–52]

$$k_{\text{uni}} = \kappa(T)\frac{\sigma k_B T}{h}\frac{Q^{\dagger}_{TS}(T)}{Q_A(T)}\exp(-E_a/RT), \quad (6)$$

where k_B, h, and R represent the Boltzmann's, Planck's, and the ideal gas constants, respectively. In the above equation, σ is the reaction-path degeneracy, $Q^{\dagger}_{TS}(T)$ and $Q_A(T)$ correspond to the total partition functions of the transition state and the reactant, and $\kappa(T)$ denotes a tunneling correction factor, which has been calculated by means of the asymmetric Eckart model [53, 54].

According to RRKM theory, the energy-dependent microcanonical rate constants, $k(E)$, for the unimolecular decomposition of a molecule with internal energy E can be expressed as [55]

$$k(E) = \frac{\sigma\, G^{\dagger}(E - E_o)}{h\, N(E)}. \quad (7)$$

In the above equation, $G^{\dagger}(E–E_o)$ is the sum of transition states density of states at an energy ranging from 0 to $E–E_o$, where E_o is the critical energy for the reaction, and $N(E)$ is the density of vibrational states in the activated molecule at an energy E. $G^{\dagger}(E–E_o)$ and $N(E)$ were computed using the Beyer–Swinehart exact counting algorithm [56] improved by Stein and Rabinovitch [57]. Canonical (temperature dependent) RRKM rate constants were determined from state integration and Boltzmann averaging.

TST and RRKM kinetic rate constants for the unimolecular decomposition of compounds **1**–**3** were obtained using the KiSThelP program [58]. A one-dimensional Eckart potential energy barrier has been used to account for quantum–mechanical tunneling effects [53, 54]. The strong collision approximation has been used. It has been assumed that every collision deactivates the molecule with $\omega = \beta_c \cdot Z_{LJ} \cdot [M]$ corresponding to the effective collision frequency, along with β_c the collisional efficiency, $[M]$ the total gas concentration, and Z_{LJ} the Lennard–Jones (LJ) collision frequency. The collision frequencies (Z_{LJ}) were computed from the LJ parameters. The employed LJ potential

Table 8 Lennard–Jones (LJ) potential parameters

Species	LJ potential parameters	
	σ/Å	ε/k_B/K
Argon	3.465	113.5
Allyl methyl amine (**1**)	5.3	406.3
Allyl methyl ether (**2**)	5.2	378.8
Allyl methyl sulfide (**3**)	5.4	438.2

parameters for argon (as diluent gas) [59] and the reactants [60] are listed in Table 8.

References

1. Vitins P, Egger KW (1974) J Chem Soc Perkin Trans 2:1289
2. Egger KW, Vitins P (1974) Int J Chem Kinet 6:429
3. Kwart H, Sarner SF, Slutsky J (1973) J Am Chem Soc 95:5234
4. Martin G, Ropero M, Avila R (1982) Phosphorus Sulfur Relat Elem 13:213
5. Eyring H (1935) J Chem Phys 3:107
6. Johnston HS (1966) Gas phase reaction rate theory. Roland Press, New York
7. Laidler KJ (1969) Theories of chemical reaction rates. McGraw-Hill, New York
8. Weston RE, Schwartz HA (1972) Chemical kinetics. Prentice-Hall, New York
9. Rapp D (1972) Statistical mechanics. Holt, Rinehart, and Winston, New York
10. Nikitin EE (1974) Theory of elementary atomic and molecular processes in gases. Clarendon Press, Oxford
11. Smith IWM (1980) Kinetics and dynamics of elementary gas reactions. Butterworths, London
12. Reed AE, Curtiss LA, Weinhold F (1988) Chem Rev 88:899
13. Zhao Y, Truhlar DG (2008) Theor Chem Acc 120:215
14. Dunning TH (1989) J Chem Phys 90:1007
15. Robinson PJ, Holbrook KA (1972) Unimolecular reactions. Wiley, New York
16. Steinfeld JI, Francisco JS, Hase WL (1999) Chemical kinetics and dynamics. Prentice-Hall, Englewood Cliffs
17. Eyring H, Lin SH, Lin SM (1980) Basic chemical kinetics. Wiley, New York
18. Reed AE, Weinstock RB, Weinhold F (1985) J Chem Phys 83:735
19. Badenhoop JK, Weinhold F (1999) Int J Quantum Chem 72:269
20. Hammond GS (1953) J Am Chem Soc 77:334
21. Agmon N, Levine RD (1977) Chem Phys Lett 52:197
22. Bickelhaupt FM, Houk KN (2017) Angew Chem Int Ed 56:10070
23. Ess DH, Houk KN (2007) J Am Chem Soc 129:10646
24. Legault CY, Garcia Y, Merlic CA, Houk KN (2007) J Am Chem Soc 129:12664
25. Ess DH, Houk KN (2008) J Am Chem Soc 130:10187
26. Hayden AE, Houk KN (2009) J Am Chem Soc 131:4084
27. Schoenebeck F, Ess DH, Jones GO, Houk KN (2009) J Am Chem Soc 131:8121
28. van Zeist W-J, Bickelhaupt FM (2010) Org Biomol Chem 8:3118
29. Fernández I, Cossío FP, Bickelhaupt FM (2011) J Org Chem 76:2310
30. Fernández I, Bickelhaupt FM (2012) J Comput Chem 33:509
31. Fernández I, Bickelhaupt FM, Cossío FP (2012) Chem Eur J 18:12395
32. Fernández I, Cossío FP, Sierra MA (2009) Chem Rev 109:6687
33. Fernández I, Bickelhaupt FM, Cossío FP (2014) Chem Eur J 20:10791
34. Fernández I, Bickelhaupt FM (2014) Chem Soc Rev 43:4953
35. Ziegler T, Rauk A (1977) Theor Chim Acta 46:1
36. Ziegler T, Rauk A (1979) Inorg Chem 18:1558
37. Bickelhaupt FM, Ziegler T, von Rague Schleyer P (1995) Organometallics 14:2288
38. Lendvay G (1989) J Phys Chem 93:4422
39. Wiberg KB (1968) Tetrahedron 24:1083
40. Glendening ED, Reed AE, Carpenter JE, Weinhold F (1998) NBO Version 3.1. Theoretical Chemistry Institute and Department of Chemistry, University of Wisconsin, Madison
41. Moyano A, Periclas MA, Valenti E (1989) J Org Chem 54:573
42. Rosas F, Dominguez RM, Tosta M, Mora JR, Marquez E, Cordova T, Chuchani G (2010) J Phys Org Chem 23:743
43. Knippenberg S, Bohnwagner MV, Harbach PH, Dreuw A (2015) J Phys Chem A 119:1323
44. Chai JD, Head-Gordon M (2008) Phys Chem Chem Phys 10:6615
45. Shiroudi A, Deleuze MS (2015) J Mol Model 21:301
46. Frisch MJ, Trucks GW, Schlegel HB, Scuseria GE, Robb MA, Cheeseman JR, Scalmani G, Barone V, Mennucci B, Petersson GA, Nakatsuji H, Caricato M, Li X, Hratchian HP, Izmaylov AF, Bloino J, Zheng G, Sonnenberg JL, Hada M, Ehara M, Toyota K, Fukuda R, Hasegawa J, Ishida M, Nakajima T, Honda Y, Kitao O, Nakai H, Vreven T, Montgomery JA Jr, Peralta JE, Ogliaro F, Bearpark M, Heyd JJ, Brothers E, Kudin KN, Staroverov VN, Kobayashi R, Normand J, Raghavachari K, Rendell A, Burant JC, Iyengar SS, Tomasi J, Cossi M, Rega N, Millam JM, Klene M, Knox JE, Cross JB, Bakken V, Adamo C, Jaramillo J, Gomperts R, Stratmann RE, Yazyev O, Austin AJ, Cammi R, Pomelli C, Ochterski JW, Martin RL, Morokuma K, Zakrzewski VG, Voth GA, Salvador P, Dannenberg JJ, Dapprich S, Daniels AD, Farkas O, Foresman JB, Ortiz JV, Cioslowski J, Fox DJ (2009) Gaussian 09, Revision A.1. Gaussian, Inc, Wallingford
47. Parr RG, Wang W (1989) Density functional theory of atoms and molecules. Oxford University Press, New York
48. Gonzalez C, Schlegel HB (1989) J Chem Phys 90:2154
49. Gonzalez C, Schlegel HB (1990) J Phys Chem 94:5523
50. Chang R (2005) Physical chemistry for the biosciences. University Science Books, Sausalito
51. Moore JW, Pearson RG (1981) Kinetics and mechanism—the study of homogeneous chemical reactions. Wiley, New York
52. Carstensen HH, Dean AM, Deutschmann O (2007) Proc Combust Inst 31:149
53. Eckart C (1930) Phys Rev 35:1303
54. Johnson HS, Heicklen J (1962) J Phys Chem 66:532
55. Forst W (1973) Theory of unimolecular reactions. Academic Press, New York
56. Beyer T, Swinehart DF (1973) Commun Assoc Comput Mach 16:379
57. Stein SE, Rabinovitch BS (1973) J Chem Phys 58:2438
58. Canneaux S, Bohr F, Henon E (2014) J Comput Chem 35:82
59. Mourits FM, Rummens HA (1977) Can J Chem 55:3007
60. Kee RJ, Rupley FM, Miller JA, Coltrin ME, Grcar JF, Meeks E, Moffat HK, Lutz AE, Dixon-Lewis G, Smooke MD, Warnatz J, Evans GH, Larson RS, Mitchell RE, Petzold LR, Reynolds WC, Caracotsios M, Stewart WE, Glarborg P, Wang C, McLellan CL, Adigun O, Houf WG, Chou CP, Miller SF, Ho P, Young PD, Young DJ, Hodgson DW, Petrova MV, Puduppakkam KV (2010) Chemkin, Reaction design. San Diego, California